HHS Public Access

Author manuscript

Am J Transplant. Author manuscript; available in PMC 2018 July 01.

Published in final edited form as:

Am J Transplant. 2017 July ; 17(7): 1791–1801. doi:10.1111/ajt.14180.

Testing the efficacy of Contrast Enhanced Ultrasound in detecting transplant rejection using a murine model of heart transplantation

Krisztina Fischer, MD, PhD[1,2], **Shunsuke Ohori, MD**[3], **F. Can Meral, PhD**[1], **Mayuko Uehara, MD**[3], **Silvia Giannini, PhD**[4], **Takaharu Ichimura, PhD**[2], **R. Neal Smith, MD, PhD**[5], **Ferenc A. Jolesz, MD**[1], **Indira Guleria, PhD**[2], **Yongzhi Zhang, MD**[1], **Philip Jason White, PhD**[1], **Nathan J. McDannold, PhD**[1], **Karin Hoffmeister, MD**[4], **Michael M. Givertz, MD**[6], and **Reza Abdi, MD**[3]

[1]Department of Radiology, Focused Ultrasound Laboratory, Brigham and Women's Hospital, Harvard Medical School, Boston, MA, USA

[2]Renal Division and Biomedical Engineering Division, Brigham and Women's Hospital, Harvard Medical School, Boston, MA, USA

[3]Transplantation Research Center, Department of Medicine, Brigham and Women's Hospital, Harvard Medical School, Boston, MA, USA

[4]Hematology Division, Department of Medicine, Brigham and Women's Hospital, Harvard Medical School, Boston, MA, USA

[5]Department of Pathology, Massachusetts General Hospital, Harvard Medical School, Boston, MA, USA

[6]Cardiovascular Division, Department of Medicine, Brigham and Women's Hospital, Harvard Medical School, Boston, MA, USA

Abstract

One of the key unmet needs to improve long-term outcomes of heart transplantation is to develop accurate, non-invasive and practical diagnostic tools to detect transplant rejection. Early intra-graft inflammation and endothelial cell injuries occur prior to advanced transplant rejection. We developed a novel diagnostic imaging platform to detect early declines in micro-vascular perfusion (MP) of cardiac transplants using Contrast Enhanced Ultrasonography (CEUS).

The efficacy of CEUS in detecting transplant rejection was tested in a murine model of heart transplants, a standard preclinical model of solid organ transplant. As compared to the syngeneic groups, a progressive decline in MP was demonstrated in the allografts undergoing acute transplant rejection (40%, 64%, 92% on days 4, 6, and 8 post-transplantation, respectively) and

Corresponding Author: Reza Abdi, MD, Associate Professor of Medicine, Harvard Medical School, Brigham and Women's Hospital, Transplantation Research Center, EBRC, 221 Longwood Ave, 3rd Floor, Boston, MA 02115, Phone: 617-732-7249, Fax: 617-732-5254, rabdi@rics.bwh.harvard.edu.

Disclosure

The authors of this manuscript have no conflicts of interest to disclose as described by the American Journal of Transplantation.

Supporting Information

Additional Supporting Information may be found in the online version of this article.

chronic rejection (33%, 33%, 92% on days 5, 14, and 30 post-transplantation, respectively). Our perfusion studies showed restoration of MP following anti-rejection therapy, highlighting its potential to help monitor efficacy of anti-rejection therapy. Our data suggest that early endothelial cell injury and platelet aggregation contributed to the early MP decline observed in the allografts.

High-resolution MP mapping may allow for non-invasive detection of heart transplant rejection. The data presented have the potential to help in the development of next-generation imaging approaches to diagnose transplant rejection.

Introduction

Despite significant advances in transplantation, heart transplant rejection and ensuing graft loss remains a major obstacle to the long-term success of heart transplantation (1–2).

Currently, right ventricular endomyocardial biopsy remains the gold standard test for diagnosing heart transplant rejection (2–3). However, cardiac biopsy is costly and invasive with known complications (e.g., tricuspid valve damage and cardiac perforation), and has notable limitations including non-uniform distribution of rejection and marked inter-reader variability (4–6).

In response to these unmet needs, much progress has been made in developing tools for advanced gene/protein profiling in tissue, blood and urine. However, a cost-effective, non-invasive and widely available test for diagnosis of transplant rejection is still lacking (7–10). Standard imaging techniques such as serial echocardiography to assess ventricular wall thickness or ejection fraction are not sensitive enough to detect early intra-graft inflammatory responses (11).

Immediately following transplantation, endothelial cells lining the vasculature of the transplanted organ are in contact with blood borne cells of the host. Through these early interactions, donor endothelial cells actively participate in the pathogenesis of allograft rejection by creating an intra-graft inflammatory milieu (i.e., production of inflammatory cytokines) (12). In contrast to the adaptive immune cells such as T cells, which need instruction to become activated against the alloantigen, the innate immune cells (such as platelets) are already equipped in participating in these early inflammatory responses. The severity of endothelial cell injury can range from early endothelial swelling and microthrombi to severe vascular immune infiltrates, thrombosis and rupture from early to late allograft injuries (13).

Assessing microvascular perfusion (MP) of the transplanted organ for early decline in MP may allow detection of early microvascular injury as a sensitive predictor of allograft rejection. To accurately assess MP, we used Contrast Enhanced Ultrasonography (CEUS), in combination with gas-filled microbubbles. With a size similar to red blood cells (1–6 μm in diameter), microbubbles remain within the vascular bed circulating in the microvasculature (14–16). CEUS was originally used to improve right heart myocardial opacification during two-dimensional echocardiography (17). However, its utility has expanded to a wide variety of molecular imaging techniques, drug delivery and tissue engineering (15). When exposed

to ultrasound pulses, circulating microbubbles in the microvasculature expand and contract generating strong echoes distinguishable from the echoes emitted from the surrounding peripheral tissue. In addition, applying a high intensity ultrasound pulse to burst the microbubbles in a selected field, and subsequently monitoring the time and intensity by which microbubbles are resumed in the microvasculature can yield further information regarding the microvasculature patency. One of the emerging applications of CEUS is to assess the MP of tissues (18–24). Nonetheless, the application of CEUS in the diagnosis of transplant rejection remains to be fully explored. Assessing MP of the entire organ in high-resolution would be particularly important in the case of heart transplant rejection as the lesions are commonly reported to be patchy (25–26). Past efforts have demonstrated that distinguishing between signal and noise while trying to provide pixel-by-pixel analysis of MP of the entire organ is a challenging task (22). Novel approaches to map MP with high spatial detail in organ transplantation may open new avenues in early transplant rejection detection.

Here, we used a high-resolution parametric perfusion map of CEUS signals to depict MP abnormalities in the transplanted organ. We focused on the pathogenic role of platelets as early recruiting cells to activated endothelium, which may explain early reduction in MP proceeding graft rejection.

Materials and Methods

Mice

C57BL6/J (H-2b), BALB/c (H-2d) and B6.C-H2bm12/KhEg (BM12) mice were purchased from the Jackson Laboratory, Bar Harbor, ME, USA. All animals were housed in accordance with Institutional and National Institutes of Health guidelines. All animal experiments were approved by the Harvard Medical School Animal Management Committee.

Murine cardiac transplantation

The vascularized cardiac grafts were transplanted intra-abdominally using microsurgical techniques as described previously by us (27). The survival of cardiac allografts was assessed by daily palpation. Rejection was defined as cessation of cardiac contractility and confirmed by histological examination.

Platelet depletion

Adsorbed Rabbit anti-Mouse Platelet Serum (RAMPS) for reducing circulating platelet was purchased from Cedarlane (Ontario, CANADA). Twenty-five microliter of RAMPS was injected into recipient mice intra-peritoneally, one day after cardiac transplantation. Transplanted hearts were harvested at day 4 post-cardiac transplantation in the acute model and at day 5 post-cardiac transplantation in the chronic model.

Antibodies, reagents and microbubble contrast agent

Anti-CD3 antibodies for treating acute rejection were purchased from BD Biosciences (San Jose, CA, USA). For platelet inhibition, cardiac allograft recipients were treated with integrin αvβ3 antagonist (cRGD) Cyclo [Arg-Gly-Asp-D-Phe-Val] (Enzo Life Sciences,

Farmingdale, NY, USA), 50 μg b.i.d, i.p. on days 0, 1, 2, 3 and 4 post-transplantation. A microbubble-based contrast agent (MicroMarker, Bracco Spa, Milan, Italy) was administered via the tail vein as an intermittent infusion at 13 μl/min.

CEUS imaging technique

The ultrasound transducer was placed on the transplanted heart (open at mid-abdomen). The transducer position was fixed using a mechanical positioning system. Non-linear contrast imaging was performed with a small-animal ultrasound scanner (Vevo 2100, VisualSonics, Toronto, Canada) using a broadband linear transducer array (13–24 MHz, MS250, VisualSonics). B-mode images were used to initially locate the graft and to optimally position the transducer over the imaging plane. MicroMarker contrast agent was infused at the rate of 13 μl/min for approximately 4 min, with a maximum dose of 65 μl per animal. A destruction-reperfusion sequence was used for the estimation of MP. Non-linear contrast images were acquired based on the principle of amplitude modulation. During image acquisition the “steady-state” level was visually determined and it was usually achieved in 80 s. High Mechanical Index (MI=0.8, line density 512) pulses were delivered to burst the contrast agents. Refilling was observed at low MI (MI=0.11, acquired at Frame Rate = 25 Hz for 32 s, 800 frames). The imaging plane was moved horizontally through the graft’s axis to have three representative cross-sectional images. Digital cine loops of all imaging data were acquired uniformly throughout the experiments from the initiation of the contrast agent infusion to the last refilling sequence. The animal’s heart rate was monitored throughout the experiment to ensure stable hemodynamic conditions.

Image processing and analysis

Audio Video Interleave (AVI) files were acquired at each pixel’s intensity as described previously (24). A Levenberg-Marquardt algorithm, which is suitable for non-linear data fitting problems, was used to solve for the perfusion parameters. Regions of interest (ROI) corresponding to the myocardium were manually extracted for analysis from B-mode images using cubic spline interpolation of user-defined boundary points. The corresponding contrast images for each ROI were spatially averaged to yield a single time-curve. Artificially hyper-echogenic regions and regurgitations in large vessels (consequence of the transplant surgery) were excluded from the ROI selection. A 25-point median filter was applied at multiple stages to the time series in order to mediate motion artifacts (respiratory or bulk motion) and increase the signal-to-noise ratio of single-pixel data for high spatial resolution perfusion mapping.

Histology, Immunohistochemistry and Immunofluorescence

Grafts were embedded in paraffin or Tissue-Tek OCT Compound (Sakura Finetek, Torrance, CA, USA) and frozen. Paraffin sections were stained with hematoxylin and eosin (H&E), as well as for von Willebrand factor (vWF) using Leica Bond Polymer Refine detection kit (Leica Microsystems Inc., Buffalo Grove, IL, USA) and rabbit polyclonal antibody in 1:400 dilution (vWF antibody, Dako North America, Carpinteria, CA, USA) raised against mice and human vWF. Trichrome staining was used to visualize fibrotic tissue in the transplanted grafts. Verhoeff’s elastic stain was used to demonstrate the elastic fibers in the arterial and arteriolar vessel wall. Immunofluorescence staining was performed on OCT-embedded

tissues sections. Platelets were stained using the platelet specific rat anti-mouse CD42b (GPIbα Emfret Analytics, Eibelstadt, Germany). Endothelial cells were stained with the endothelium specific goat anti-mouse endoglin (Millipore, Billerica, MA) or rabbit anti-mouse vWF (Emfret Analytics, Eibelstadt, Germany) antibodies. Goat anti-rat AlexaFluor 568, goat anti-mouse AlexaFluor 488 or goat anti-rabbit AlexaFluor 488 (Life Technologies, Grand Island, NY, USA) were used as secondary antibodies. The fluorophore-conjugated anti-CD3 and F4/80 macrophage antibodies were purchased from eBioscience (San Diego, CA, USA) and ATCC (Manassas, VA, USA). Sections were then mounted with anti-fade medium with DAPI (Life Technologies, Grand Island, NY, USA) and analyzed using a FluoView FV-10i Olympus Laser Point Scanning Confocal Microscope (Olympus, Center Valley, PA, USA). The % of area covered by platelets was quantified using Image J in five different fields in each sample.

Histology scores

Four sections of H&E from one heart were observed for histological scoring (4 sections/heart, 3 mice per group). For lymphocyte infiltration scoring, each one section of heart was divided into 6 parts, and lymphocyte infiltration was graded using a scale modified from the International Society for Heart and Lung Transplantation (0, no lymphocyte infiltration; 1, less than 25% lymphocyte infiltration; 2, 25 to 50% lymphocyte infiltration; 3, 50 to 75% lymphocyte infiltration; 4, more than 75% lymphocyte infiltration with hemorrhage and/or necrosis) for each part, then taken average of 6 parts for one section. The average from four sections was used as lymphocyte infiltration score of observed heart. The severity of vasculopathy was determined by a combination of vascular occlusion score and perivascular lymphocyte infiltration score for each vessel, and the average was taken. Vascular occlusion was scored from grade 0 to 3. The grades were defined as follows: grade 0 (no or minimal <10%), grade 1 (10–50% occlusion), grade 2 (50% to 75% occlusion) and grade 3 (more than 75% occlusion). The perivascular lymphocyte infiltration was scored as grade 0 (no lymphocyte infiltration), grade 1 (mild lymphocyte infiltration), 2 (moderate lymphocyte infiltration) and 3 (severe lymphocyte infiltration and then added to the vascular occlusion score (final score is from 0 to 6).

Electron microscopy (EM)

Tissue was fixed in Karnovsky's glutaraldehyde-based fixative and stored at 4°C and processed using standard methods. Toluidine blue-stained sections of plastic embedded tissue were examined to select areas for ultrastructural review, which was done on a FEI Morgani electron microscope. Images were captured using AMT Advanced Microscopy 2K CCD Digital Camera.

Statistical analysis

Student's *t*-test was used to determine significant differences. A p value of less than 0.05 was considered to be significant. Results are expressed as means ± S.D. SPSS 21 (IBM, Armonk, NY, USA) was used for statistical analysis.

Results

Detecting acute heart allograft rejection using high-resolution parametric MP mapping

Heart transplants were performed in two groups of syngeneic (C57BL6/J hearts into C57BL6/J recipients) and allogeneic recipients (BALB/c into C57BL6/J recipients). CEUS images were acquired following MicroMarker contrast agent administration. High-resolution perfusion maps showed a gradual decrease in the allograft perfusion on days 4, 6 and 8 post-transplantation as compared to syngeneic grafts (Figure 1A). Parametric maps show signal intensity change over 800 frames for each imaging series. Red and yellow colors represent higher echo intensity change and higher MP, respectively, whereas dark blue indicates no perfusion. By day 8 post-transplantation, MP was measurable in allogeneic grafts only in the septum and the epicardial layer of the left ventricle, while in the syngeneic grafts, no significant changes were found in the MP throughout the 8-day imaging period (Figure 1A). In addition, no significant difference was found between the animal's heart rate in the individual experimental groups (data not shown).

Perfusion analysis strongly correlated with the histology data of acute cellular rejection. In the allogeneic group, mild inflammation was evident on day 4 post-transplantation, with progression toward end stage rejection—cellular infiltrates, massive bleeding and development of vascular thrombi—by day 8 (Figure 1B). Additionally, the CD3 immunostaining showed progressive infiltration of CD3 positive T-lymphocytes, which also peaked on day 8 post-transplantation (Figure S1A). A similar trend was observed with F4/80 positive macrophage infiltration (Figure S1B).

Once the microbubbles saturated the contrast image, a high mechanical index (MI) was delivered to burst the bubble. As the contrast re-perfused in the organ transplant, the average plateau intensity values were then calculated. In the acute rejection model, perfusion curves confirmed a sharp and progressive decrease in MP in allogeneic animals on days 4, 6 and 8 post-transplantation (Figure 1C). In syngeneic animals, the graft myocardium perfusion did not change significantly between the different days of imaging (Figure 1C). In allogeneic grafts, average echo intensity index (units±SD) on days 4, 6, and 8 post-transplantation were 14±3, 10±6.5 and 1.8±2.7 as compared to 23±6.5, 28±14 and 23±5 in the syngeneic grafts, respectively (Figure 1D, n=3–5, $p<0.05$). These results indicate that MP levels in allogeneic grafts were lower by 40%, 64%, and 92% on days 4, 6 and 8 post-transplantation, respectively, when compared to syngeneic grafts. The early accumulation of platelets in vessels in response to potential ischemia-reperfusion injury was tested in syngeneic and allogeneic grafts on day 2. There was no platelet adhesion on the vessels at this early time point (data not shown).

Utility of CEUS in monitoring the effects of allograft rejection therapy

Cardiac allograft recipients were treated with anti-CD3 antibody (100 μg i.p.) on day 4 post-transplantation. Figure 2A shows the parametric perfusion maps of the anti-CD3 treated and untreated animals on days 6 and 8 post-transplantation. Heart allograft recipients treated with anti-CD3 antibody showed resolution of MP impairment as compared to allografts from untreated recipients, which showed marked reduction in MP in the entire graft (the only

measurable perfusion was in the septal area). Figure 2B and C show the histological analysis of the cell infiltration and vasculopathy scores in syngeneic, allogeneic and anti-CD3 treated allogeneic grafts. Following anti-CD3 treatment heart allografts showed significantly reduced cell infiltration and vasculopathy scores as compared to non-treated allografts, which showed great increase in cell infiltration and vasculopathy scores over time (day 4, 6 and 8 post-transplantation). A strong correlation was found between the MP and the cell infiltration score ($R=-0.74$, $p=0.02$); and MP and vasculopathy score ($R=-0.82$, $p=0007$) in non-treated allografts.

Early platelet accumulation in allografts

The paucity of lymphocytic and macrophage infiltrates in the heart allografts in early post-transplant rejection (day 4 post-transplantation) was contrasted with the reduction in perfusion as early as day 4. We tested the hypothesis that early platelet aggregation and microvascular injuries, such as endothelial swelling and microperfusion, might have contributed to the early MP defects in the allogeneic grafts. Sections of the hearts were stained for platelets and vWF. In allografts, we found numerous platelets, accumulated to the sub-epicardial vessel wall with close proximity to endoglin and vWF positive-endothelial cells. Electron microscopic ultrastructural analysis showed that platelets accumulated intracapillary only in the allogeneic grafts. In contrast, syngeneic grafts showed no platelet accumulation in the capillaries (Figure 3A). As shown in Figure 3B, there was a significantly greater platelet infiltrate in the allografts as compared to syngeneic grafts (1.9±0.6 vs. 0.06 ±0.04 % area covered by platelets in the allogeneic vs. syngeneic grafts respectively, $p<0.01$, $n=3$ in each group).

To show the functionality of platelet aggregation or accumulation as a contributor to the decline in MP, we performed heart transplants and treated the recipients with an integrin inhibitor cRGD (Cyclo [Arg-Gly-Asp-D-Phe-Val]), which has been shown to interfere with platelet adhesion (28). Figure 3C shows the parametric perfusion maps of the anti-cRGD (integrin inhibitor) treated and untreated allogeneic grafts on day 4 post-transplantation. The anti-cRGD-treated allogeneic grafts showed much better MP than untreated allogeneic grafts (average echo intensity index (units ±SD) on day 4 post-transplantation, 31±10 vs. 15±4, respectively, $n=3$, $p<0.05$; Figure 3D).

In order to further support the role of platelet in MP decline during acute rejection, we depleted the platelets with an anti-platelet antibody (RAMPS), which showed marked reduction of platelet post-treatment. (Figure 3E). Figure 3F shows the average MP in untreated syngeneic, platelet depleted and allogeneic allografts (n=3–5). The MP was significantly lower in the untreated allografts as compare to platelet depleted graft perfusion (average echo intensity index (units ±SD) on day 4 post-transplantation, 14±3 vs. 25±1, respectively). There was no difference in MP between the platelet depleted and syngeneic groups.

Utility of parametric high-resolution perfusion mapping in detecting chronic heart allograft rejection

We then evaluated the ability of our imaging platform to detect chronic cardiac allograft rejection, which is a major barrier to long-term survival following heart transplantation. We used a single MHC mismatch model (BM12 hearts into C57BL6/J recipients) as described previously (29–30). We imaged the transplanted hearts on days 5, 14 and 30 post-transplantation to assess MP with high spatial and temporal resolution. Parametric perfusion maps depicted a decline in perfusion as early as day 5 post-transplantation (Figure 4A). The MP decreased significantly in the allogeneic grafts over time from days 5 to day 30 post-transplantation as compared to the syngeneic grafts, which did not show a decline over time (Figure 4A). Correlating with our perfusion maps, histological examination of heart allografts demonstrated cellular infiltration and increased vWF expression (Figures 4B and 4C). Immunophenotyping showed a progressive accumulation of CD3 lymphocytes (Figure S2A) and F4/80 positive macrophages over time (Figure S2B). The control (syngeneic) graft did not demonstrate such inflammatory responses (Figure 4B and C, Figure S2A and S2B).

We also evaluated the plateau intensity values, which indicated significant MP decrease (Figure 4D) in the whole allograft. The average MP index in the myocardium of the chronic allograft rejection model was substantially less than in the syngeneic grafts (18±6, 17±6 and 3±2 vs. 26±3, 25±3 and 36±3 units at days 5, 14 and 30, respectively; n=3–4, $p<0.05$), indicating that the MP decreased by 33%, 33% and 92%, respectively (Figure 4E). The MP maps showed a steady level of perfusion from the time of transplantation to day 30 post-transplantation in syngeneic grafts. Notably, our MP study showed a decline in perfusion at day 5 post-transplant at a time point when histology did not show marked changes indicative of chronic rejection. The classical histological evidence of chronic rejection was observed around day 30 post-transplant.

We also used similar platelet depletion strategy in our chronic rejection model to examine the role of platelet as a contributor to the decline in MP seen in our heart grafts. The average MP in untreated allografts was 18±6 as compare to 26±3 in platelet depleted grafts (average echo intensity index (units ±SD) on day 5 post-transplantation, n=3–4, $p<0.05$). There was no difference found in MP between the platelet depleted and syngeneic grafts (Figure S2C).

Discussion

Heart transplantation has emerged as a routine life-saving strategy for patients with end-stage heart disease. About 14% of heart transplant recipients experience a treated episode of rejection within the first year. The incidence of chronic rejection increases over time in cardiac transplant patients with approximate incidence time of ~40% at 5 years post transplant (31–33). Similar rates of transplant rejection have also been reported using other organs such as kidneys (34). Organ transplant biopsies remain the gold standard for diagnosing allograft rejection in solid organ transplantation, but are invasive, costly and carry significant risks (4, 35). Furthermore, biopsy lacks sensitivity due to sampling error; suffer from significant variability in reporting the pathological results. Importantly, histological lesions required to define graft rejection typically determine established lesions and may not allow application of early intervention (25, 36, 37). These limitations

underscore the need for a diagnostic test for heart transplant rejection that is non-invasive, accurate, and cost-effective for widespread clinical use. There have been major efforts to develop biomarkers (using gene expression and protein profiling) as a non-invasive method for the diagnosis of allograft rejection. However, due to many limitations (including non-reproducibility, cost, and impracticality), these techniques have not been fully integrated into clinical practice. Here, we report developing a novel imaging platform that not only correlates strongly with both acute and chronic rejection, but also has the potential to identify patients at risk for rejection and assess the efficacy of anti-rejection therapy.

Endothelial cells are the interface between host immune responses and the organ itself. Early post-transplantation endothelial cell injuries initiate potent intra-graft inflammatory responses, which subsequently augment adaptive immune responses. Early endothelial injuries have been the precursors to overt atherosclerotic lesions as well as cardiac allograft vasculopathy (38). Classical pathological manifestations of graft rejection rely heavily on the presence of adaptive immune cells (such as T cell infiltrates) that are late players of graft rejection (39). The biological markers representative of early innate immune activation are lacking in traditional pathological examination. Indeed, our data indicate that at an early post-transplant stage, prior to advanced lymphocytic infiltration, there is marked endothelial cell swelling with platelet aggregation. While adaptive immune cells such as T cells require instruction, innate immune cells, on the other hand, are fully prepared for early participation in inflammatory responses. Emerging studies highlight platelets as the most potent amongst innate immune cells. Platelets can participate actively in the inflammatory process through secretion of pro-inflammatory molecules interacting with endothelial cells (40). The accumulation of platelets and fibrin during rejection of renal transplants has long been demonstrated (41–42). Nonetheless, the implication of platelets in transplant rejection remains under explored as the primary focus of transplant research has been on adaptive immune cells. The importance of platelets in the pathogenesis of graft rejection has been recognized by a number of studies; such as they enhance the recruitment of inflammatory cells (43–44). Studying polymorphisms of the ITGB3 gene encoding β3 integrin (important in platelet junction) could identify patients at risk for renal transplant rejection (45). Our study not only emphasizes the role of platelets in early vascular inflammation, but also stresses the importance of further examining the role of platelets in allograft rejection and treatment.

In contrast to prior studies where MP was estimated over a subjectively selected region of interest using CEUS, our study used a custom designed algorithm, which provided high-resolution MP estimation based on plateau image intensity data (18–23). The high-resolution, pixel-by-pixel parametric perfusion maps indicated subtle, regional dysfunction in graft perfusion earlier than seen with histology, suggesting that the method can be used as a truly early diagnostic modality. The high-resolution parametric perfusion maps allow depiction of early regional perfusion dysfunction, which is especially relevant in organ rejection, because of the irregular appearance of the immune response.

Our study focuses on a high resolution imaging technology to readily assess the status of the microvasculature early on post solid organ transplantation. We used a murine model of heart transplant, which is the most widely used model to study solid organ transplant rejection.

The rate and timing of rejection is highly predictable in this model, which makes it an ideal one to corroborate with imaging data.

In future studies, we plan to examine the importance of CEUS in further differentiating the causes of early allograft dysfunction, including the types of rejection (cellular vs. antibody-mediated), prolonged ischemia and/or calcineurin inhibitor toxicity. It is likely that the pattern of MP defect varies amongst these conditions. These studies may require more targeted imaging together with CEUS. Our microbubble has a lipid shell. Several generations of microbubbles have been developed using various shell-stabilizing materials including albumin and phospholipid (46). While lipid-based microbubbles display longer half-life, their superiority to albumin-based shells remain to be explored, especially given that the events to be measured occur within seconds. Lipid-based microbubbles might be uptaken by large numbers of macrophages harbored within the rejected grafts. This may constitute an interesting approach of using lipid-based microbubbles for targeted imaging.

There are a number of studies that used microbubbles with targeted ligands for adhesion molecules that accumulate at the sites of injury (47–50). However, the expression of these molecules could change due to a number of variables, including the type and potency of immunosuppressive agents used in different transplant cohorts. Although it remains to be proven, our high-resolution perfusion mapping using CEUS represents a powerful tool to assess microvascular inflammation that is shared by allograft rejection across populations and organs. Our diagnostic platform may allow the detection of early allograft inflammation before even the targeted molecules are significantly upregulated. Endothelial interaction with leukocytes and resulting microvascular inflammation is a universal pathological feature of organ rejection. This imaging platform could allow clinicians to apply early interventions before the development of advanced organ lesions. Finally, the high-resolution perfusion maps has the potential to detect restoration in MP following anti-rejection therapy. These studies may allow tailoring of the intensity and duration of therapies, which are currently carried out blindly.

Lastly, our study could potentially guide clinicians to obtain tissue from specific sites where perfusion is reduced and thereby reduce sampling error. Contrast agents are FDA approved and currently available for imaging left ventricular structure and function at rest and during stress (51). Given the safety profile of microbubbles and its easy-to use feature, CEUS could be integrated into the widespread standard of care of heart transplant patients (52). Much works need to be carried out to dissect the impacts of other factors which could alter the MP such as the effect of calcinurin inhibitors or ischemia reperfusion injuries. It would be of interest to examine the pattern of MP defects in these settings comparing with the ones of transplant rejection. Whether such technology allows differentiation between humoral and cellular rejection is a highly interesting subject, which deserves attention. In future studies, we will also examine the utility of this technique in assessing the robustness of tolerogenic transplant protocols.

In summary, our novel imaging platform has the clinical potential to greatly improve the outcome of heart transplantation by enabling physicians to predict, diagnose and monitor treatment of acute and chronic forms of transplant rejection.

Supplementary Material

Refer to Web version on PubMed Central for supplementary material.

Acknowledgments

We thank VisualSonics (Toronto, Canada) for providing the MicroMarker contrast agent for this research project. Authors are very grateful for Fred Roberts and Dr. Sudeshna Fisch for their generous assistance in the experiments.

The preparation of this manuscript has been overshadowed by Dr. Jolesz' sudden passing in December 2014. The goals of this work and the composition of the paper were written jointly and we have done our best to complete them. In sorrow we dedicate this work to his memory.

This work was supported in part by NIH grants R01AI126596-01 (R.A), 4R25CA089017-14 (K.F), 5P41EB015898-12 (K.F).

Abbreviations

MP	Micro-vascular perfusion
CEUS	Contrast enhanced ultrasonography
MI	Mechanical Index
AVI	Audio Video Interleave
ROI	Regions of interest
H&E	Hematoxylin and eosin
vWF	von Willebrand factor
EM	Electron microscopy

References

1. Hunt SA, Haddad F. The changing face of heart transplantation. J Am Coll Cardiol. 2008; 52(8): 587–598. [PubMed: 18702960]
2. Usta E, Burgstahler C, Aebert H, Schroeder S, Helber U, Kopp AF, Ziemer G. The challenge to detect heart transplant rejection and transplant vasculopathy non-invasively - a pilot study. J Cardiothorac Surg. 2009; 4:43. [PubMed: 19682394]
3. Costanzo MR, Dipchand A, Starling R, Anderson A, Chan M, Desai S, et al. The International Society of Heart and Lung Transplantation Guidelines for the care of heart transplant recipients. J Heart Lung Transplant. 2010; 29(8):914–956. [PubMed: 20643330]
4. Baraldi-Junkins C, Levin HR, Kasper EK, Rayburn BK, Herskowitz A, Baughman KL. Complications of endomyocardial biopsy in heart transplant patients. J Heart Lung Transplant. 1993; 12(1 Pt 1):63–67. [PubMed: 8443204]
5. Marboe CC, Billingham M, Eisen H, Deng MC, Baron H, Mehra M, et al. Nodular endocardial infiltrates (Quilty lesions) cause significant variability in diagnosis of ISHLT Grade 2 and 3A rejection in cardiac allograft recipients. J Heart Lung Transplant. 2005; 24(7 Suppl):S219–226. [PubMed: 15993777]
6. Tan CD, Baldwin WM 3rd, Rodriguez ER. Update on cardiac transplantation pathology. Arch Pathol Lab Med. 2007; 131(8):1169–1191. [PubMed: 17683180]
7. Muthukumar T, Dadhania D, Ding R, Snopkowski C, Naqvi R, Lee JB, et al. Messenger RNA for FOXP3 in the urine of renal-allograft recipients. N Engl J Med. 2005; 353(22):2342–2351. [PubMed: 16319383]

8. Ling XB, Sigdel TK, Lau K, Ying L, Lau I, Schilling J, et al. Integrative urinary peptidomics in renal transplantation identifies biomarkers for acute rejection. J Am Soc Nephrol. 2010; 21(4):646–653. [PubMed: 20150539]
9. Jarcho JA. Fear of rejection--monitoring the heart-transplant recipient. N Engl J Med. 2010; 362(20):1932–1933. [PubMed: 20413601]
10. Pham MX, Teuteberg JJ, Kfoury AG, Starling RC, Deng MC, Cappola TP, et al. IMAGE Study Group. Gene-expression profiling for rejection surveillance after cardiac transplantation. N Engl J Med. 2010; 362(20):1890–1900. [PubMed: 20413602]
11. Lu W, Zheng J, Pan X, Sun L. Diagnostic performance of echocardiography for the detection of acute cardiac allograft rejection: a systematic review and meta-analysis. PLoS ONE. 2015; 10(3):e0121228. [PubMed: 25822627]
12. Solhjou Z, Athar H, Xu Q, Abdi R. Emerging therapies targeting intra-organ inflammation in transplantation. Am J Transplant. 2015; 15(2):305–311. [PubMed: 25612486]
13. Pober JS, Sessa WC. Evolving functions of endothelial cells in inflammation. Nat Rev Immunol. 2007; 7(10):803–815. [PubMed: 17893694]
14. Weller GE, Lu E, Csikari MM, et al. Ultrasound imaging of acute cardiac transplant rejection with microbubbles targeted to intercellular adhesion molecule-1. Circulation. 2003; 108(2):218–224. [PubMed: 12835214]
15. Kiessling F, Fokong S, Bzyl J, Lederle W, Palmowski M, Lammers T. Recent advances in molecular, multimodal and theranostic ultrasound imaging. Adv Drug Deliv Rev. 2014; 72:15–27. [PubMed: 24316070]
16. Santoso T, Roelandt J, Mansyoer H, Abdurahman N, Meltzer RS, Hugenholtz PG. Myocardial perfusion imaging in humans by contrast echocardiography using polygelin colloid solution. J Am Coll Cardiol. 1985; 6(3):612–620. [PubMed: 4031272]
17. Villanueva FS, Glasheen WP, Sklenar J, Jayaweera AR, Kaul S. Successful and reproducible myocardial opacification during two-dimensional echocardiography from right heart injection of contrast. Circulation. 1992; 85(4):1557–1564. [PubMed: 1555293]
18. Thierman JS, Clement GT, Kalish LA, O'Kane PL, Frauscher F, Paltiel HJ. Automated sonographic evaluation of testicular perfusion. Phys Med Biol. 2006; 51(14):3419–3432. [PubMed: 16825740]
19. Bulte CS, Slikkerveer J, Meijer RI, et al. Contrast-enhanced ultrasound for myocardial perfusion imaging. Anesth Analg. 2012; 114(5):938–945. [PubMed: 22366851]
20. Jin Y, Yang C, Wu S, et al. A novel simple noninvasive index to predict renal transplant acute rejection by contrast-enhanced ultrasonography. Transplantation. 2015; 99(3):636–641. [PubMed: 25119133]
21. Kalantarinia K, Belcik JT, Patrie JT, Wei K. Real-time measurement of renal blood flow in healthy subjects using contrast-enhanced ultrasound. Am J Physiol Renal Physiol. 2009; 297(4):F1129–1134. [PubMed: 19625375]
22. Schneider AG, Hofmann L, Wuerzner G, et al. Renal perfusion evaluation with contrast-enhanced ultrasonography. Nephrol Dial Transplant. 2012; 27(2):674–681. [PubMed: 21690200]
23. Schneider AG, Goodwin MD, Schelleman A, Bailey M, Johnson L, Bellomo R. Contrast-enhanced ultrasound to evaluate changes in renal cortical perfusion around cardiac surgery: a pilot study. Crit Care. 2013; 17(4):R138. [PubMed: 23849270]
24. Fischer K, Meral FC, Zhang Y, Vangel MG, Jolesz FA, Ichimura T, Bonventre JV. High-resolution renal perfusion mapping using contrast-enhanced ultrasonography in ischemia-reperfusion injury monitors changes in renal microperfusion. Kidney Int. 2016; 89(6):1388–98. [PubMed: 27165821]
25. Spiegelhalter DJ, Stovin PG. An analysis of repeated biopsies following cardiac transplantation. Stat Med. 1983; 2(1):33–40. [PubMed: 6359316]
26. Stewart S, Winters GL, Fishbein MC, et al. Revision of the 1990 working formulation for the standardization of nomenclature in the diagnosis of heart rejection. J Heart Lung Transplant. 2005; 24(11):1710–1720. [PubMed: 16297770]
27. Azzi J, Ohori Sh, Ting C, Uehara M, Abdoli R, Smith B, et al. Serine protease inhibitor-6 differentially affects the survival of effector and memory alloreactive CD8-T cells. Am J Transplant. 2015; 15(1):234–41. [PubMed: 25534448]

28. Aumailley M, Gurrath M, Muller G, Calvete J, Timpl R, Kessler H. Arg-Gly-Asp constrained within cyclic pentapeptides. Strong and selective inhibitors of cell adhesion to vitronectin and laminin fragment P1. FEBS letters. 1991; 291(1):50–54. [PubMed: 1718779]
29. Izawa A, Ueno T, Jurewicz M, et al. Importance of donor- and recipient-derived selectins in cardiac allograft rejection. J Am Soc Nephrol. 2007; 18(11):2929–2936. [PubMed: 17928506]
30. Lacy-Hulbert A, Ueno T, Ito T, Jurewicz M, Izawa A, Smith RN, Chase CM, Tanaka K, Fiorina P, Russell PS, Auchincloss H Jr, Sayegh MH, Hynes RO, Abdi R. Beta 3 integrins regulate lymphocyte migration and cytokine responses in heart transplant rejection. Am J Transplant. 2007; 7(5):1080–90. [PubMed: 17359504]
31. Okada K, Fearon WF, Luikart H, Kitahara H, Otagiri K, Tanaka S, et al. Attenuated-Signal Plaque Progression Predicts Long-Term Mortality After Heart Transplantation: IVUS Assessment of Cardiac Allograft Vasculopathy. J Am Coll Cardiol. 2016; 68(4):382–92. [PubMed: 27443435]
32. Lindenfeld J, Miller GG, Shakar SF, Zolty R, Lowes BD, Wolfel EE, Mestroni L, Page RL 2nd, Kobashigawa J. Drug therapy in the heart transplant recipient: part I: cardiac rejection and immunosuppressive drugs. Circulation. 2004; 110(24):3734–3740. [PubMed: 15596559]
33. Young JB. Perspectives on cardiac allograft vasculopathy. Curr Atheroscler Rep. 2000; 2(3):259–271. [PubMed: 11122752]
34. Chapman JR, O'Connell PJ, Nankivell BJ. Chronic renal allograft dysfunction. J Am Soc Nephrol. 2005; 16(10):3015–3026. [PubMed: 16120819]
35. Huddleston CB, Rosenbloom M, Goldstein JA, Pasque MK. Biopsy-induced tricuspid regurgitation after cardiac transplantation. Ann Thorac Surg. 1994; 57(4):832–836. discussion 836–837. [PubMed: 8166527]
36. Stewart S, Winters GL, Fishbein MC, Tazelaar HD, Kobashigawa J, Abrams J, et al. Revision of the 1990 working formulation for the standardization of nomenclature in the diagnosis of heart rejection. J Heart Lung Transplant. 2005; 24(11):1710–1720. [PubMed: 16297770]
37. Winters GL, McManus BM. Consistencies and controversies in the application of the International Society for Heart and Lung Transplantation working formulation for heart transplant biopsy specimens. Rapamycin Cardiac Rejection Treatment Trial Pathologists. J Heart Lung Transplant. 1996; 15(7):728–735. [PubMed: 8820790]
38. Colvin-Adams M, Harcourt N, Duprez D. Endothelial dysfunction and cardiac allograft vasculopathy. J Cardiovasc Transl Res. 2013; 6(2):263–277. [PubMed: 23135991]
39. Jansen MA, Otten HG, de Weger RA, Huibers MM. Immunological and Fibrotic Mechanisms in Cardiac Allograft Vasculopathy. Transplantation. 2015; 99(12):2467–75. [PubMed: 26285017]
40. von Hundelshausen P, Weber C. Platelets as immune cells: bridging inflammation and cardiovascular disease. Circ Res. 2007; 100(1):27–40. [PubMed: 17204662]
41. von Willebrand E, Zola H, Hayry P. Thrombocyte aggregates in renal allografts. Analysis with fine-needle aspiration biopsy and monoclonal antithrombocyte antibodies. Transplantation. 1985; 39(3):258–262. [PubMed: 3883591]
42. Desir G, Bia MJ, Lange RC, et al. Detection of acute allograft rejection by indium-111 labeled platelet scintigraphy in renal transplant patients. Transplantation proceedings. 1987; 19(1 Pt 2): 1677–1680. [PubMed: 3547876]
43. Kirk AD, Morrell CN, Baldwin WM 3rd. Platelets influence vascularized organ transplants from start to finish. Am J Transplant. 2009; 9(1):14–22. [PubMed: 19067663]
44. Modjeski KL, Morrell CN. Small cells, big effects: the role of platelets in transplant vasculopathy. J Thromb Thrombolysis. 2014; 37(1):17–23. [PubMed: 24264961]
45. Chandrakantan A, McDermott DH, Tran HT, et al. Role of beta3 integrin in acute renal allograft rejection in humans. Clin J Am Soc Nephrol. 2007; 2(6):1268–1273. [PubMed: 17928472]
46. Qin S, Caskey CF, Ferrara KW. Ultrasound contrast microbubbles in imaging and therapy: physical principles and engineering. Phys Med Biol. 2009; 54(6):R27–57. [PubMed: 19229096]
47. Yang H, Xiong X, Zhang L, Wu C, Liu Y. Adhesion of bio-functionalized ultrasound microbubbles to endothelial cells by targeting to vascular cell adhesion molecule-1 under shear flow. Int J Nanomedicine. 2011; 6:2043–2051. [PubMed: 21976979]

48. Takalkar AM, Klibanov AL, Rychak JJ, Lindner JR, Ley K. Binding and detachment dynamics of microbubbles targeted to P-selectin under controlled shear flow. J Control Release. 2004; 96(3): 473–482. [PubMed: 15120903]

49. Weller GE, Villanueva FS, Klibanov AL, Wagner WR. Modulating targeted adhesion of an ultrasound contrast agent to dysfunctional endothelium. Ann Biomed Eng. 2002; 30(8):1012–1019. [PubMed: 12449762]

50. Grabner A, Kentrup D, Pawelski H, Mühlmeister M, Biermann C, Edemir B, et al. Renal Contrast-Enhanced Sonography Findings in a Model of Acute Cellular Allograft Rejection. Am J Transplant. 2016; 16(5):1612–9. [PubMed: 26613381]

51. Salerno M, Beller GA. Noninvasive assessment of myocardial perfusion. Circ Cardiovascular imaging. 2009; 2(5):412–424. [PubMed: 19808630]

52. Eisenbrey JR, Sridharan A, Liu JB, Forsberg F. Recent Experiences and Advances in Contrast-Enhanced Subharmonic Ultrasound. Biomed Res Int. 2015; 2015:640397. [PubMed: 26090430]

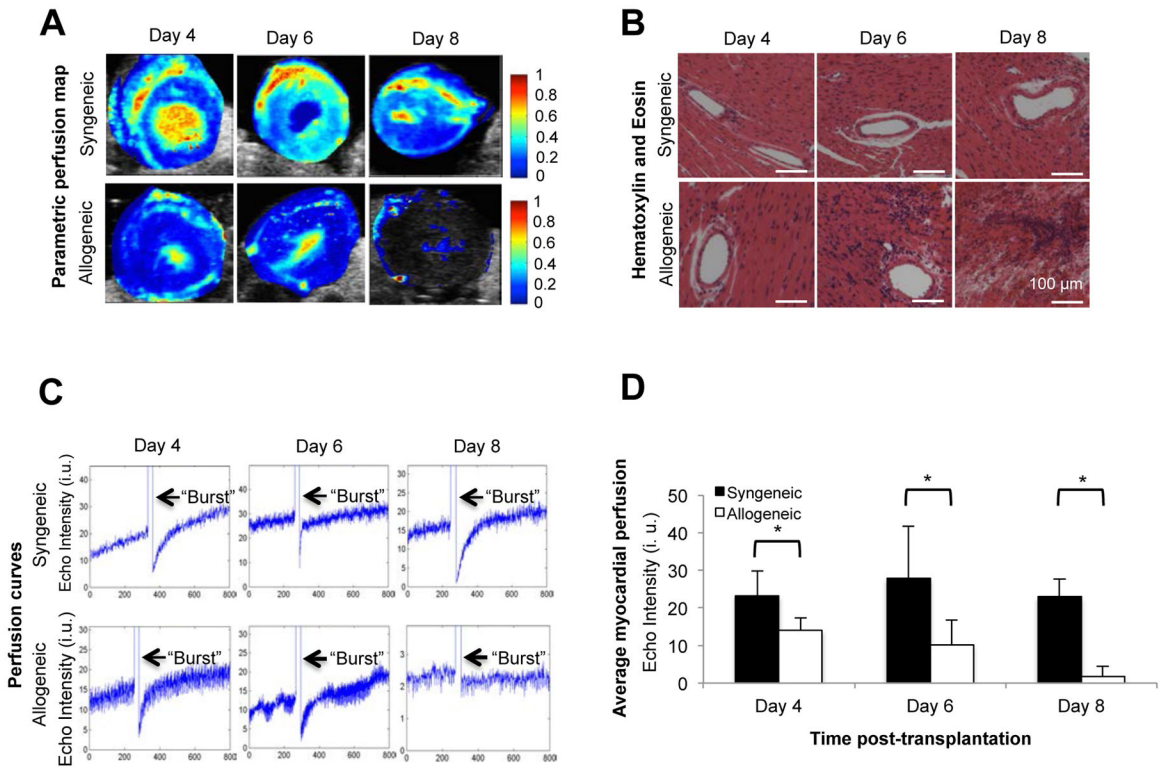

Figure 1. Use of MP mapping to detect acute heart allograft rejection

Parametric perfusion maps of syngeneic and allogeneic heart grafts show a progressive decline in tissue perfusion in the allogeneic heart grafts as compared to the syngeneic groups over time. On day 8 post-transplant, MP was markedly reduced in the allogeneic hearts. Red and yellow colors represent higher echo intensity change and higher MP (Figure 1A). H&E staining shows an increasing number of inflammatory cells infiltrating the allogeneic heart allografts over time as compared to the syngeneic groups. On day 8 post-transplant, full manifestations of acute heart transplant rejection (including massive cell infiltrate and vascular thrombi) were noted in the allogeneic graft tissue (Figure 1B). High MI pulses (arrows), which appear in the signal as a sudden increase in the echo intensity, were delivered to burst the microbubbles in the imaging plane. The intensity curves indicate lower plateau values in heart allografts as compared to syngeneic grafts. The time for reappearance of the microbubbles is longer, as represented by the lower slope of the perfusion curves in allograft compared to syngeneic grafts (Figure 1C). The diagram shows the average echo intensities for syngeneic and allogeneic grafts on day 4, 6, and 8 post-transplantation. A much higher echo intensity unit (i.u.) was observed in the syngeneic groups on each examined day as compared to the allogeneic groups (Figure 1D) (p<0.05, n=3 to 5 mice in each group).

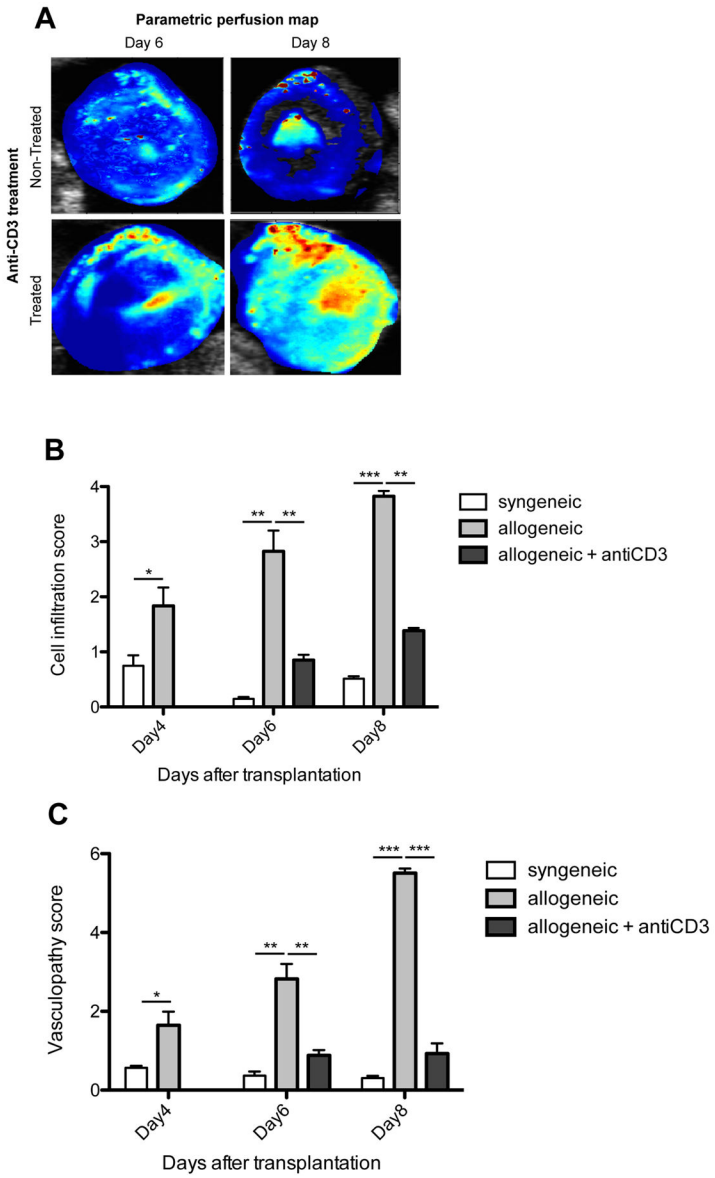

Figure 2. Utility of high-resolution perfusion mapping to monitor the effect of anti-rejection therapy

Animals treated with anti-CD3 showed higher MP on days 6 and 8 post-transplantation than untreatedcontrol animals experiencing severe graft rejection (Figure 2A). Following anti-CD3 treatment heart allografts showed reduced cell infiltration (Figure 2B) and vasculopathy scores (Figure 2C) as compared to non-treated allografts. (*): $p<0.05$, (**): $p<0.01$, (***): $p<0.001$, n=3 to 5 mice in each group.

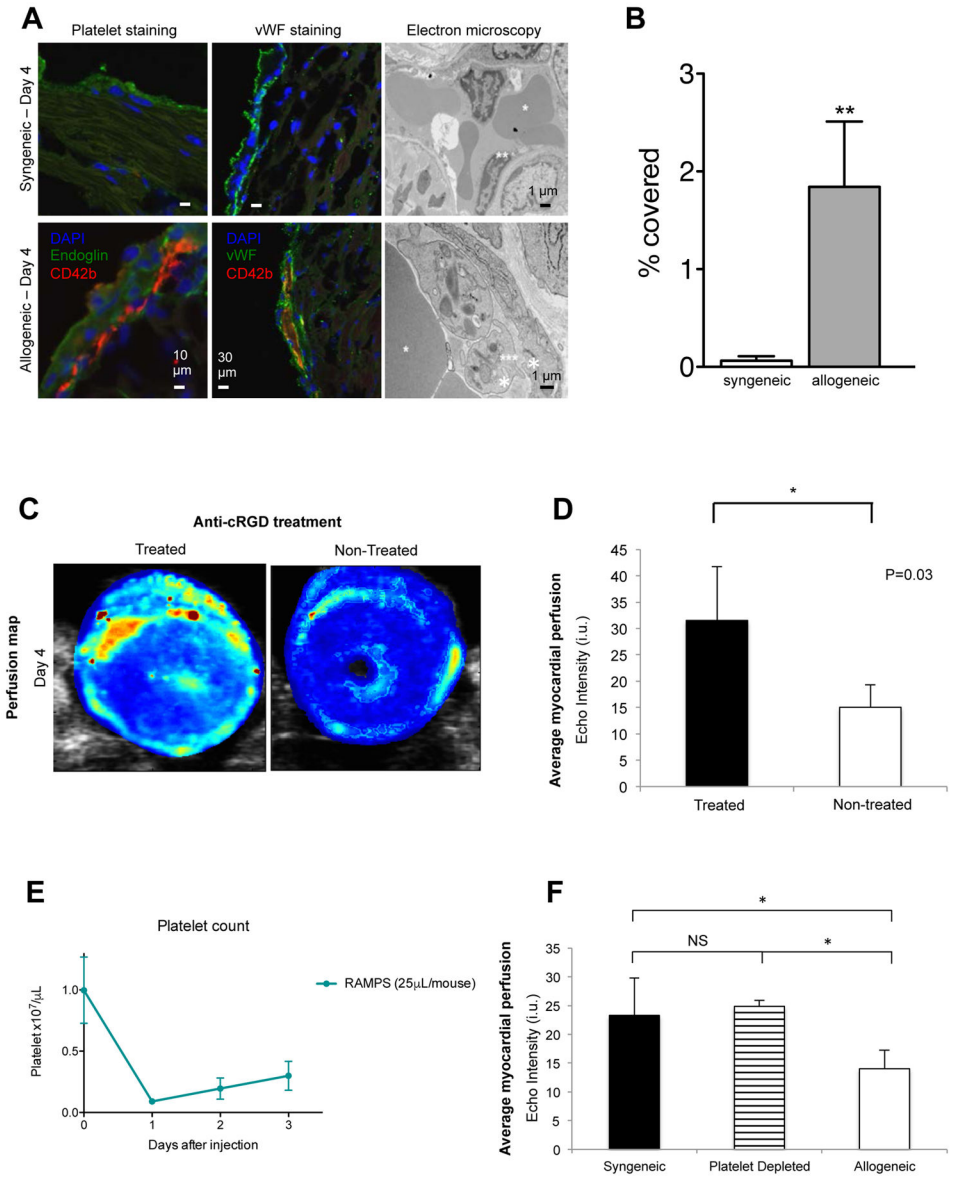

Figure 3. Early platelet accumulation in the pericardial microvasculature in the acute rejection model

Heart tissue sections of syngeneic and allogeneic grafts were stained with the platelet specific antibodies, CD42b (red) and anti-endoglin (green), or anti-vWF antibodies to visualize the endothelium (green). DAPI was used as nuclear counterstaining. On ultrastructural images of transplanted hearts platelet aggregation was found in the capillaries of the allografts. Syngeneic, original magnification, 5600x; allogeneic, original magnification, 18000x. *Red blood cell; **Endothelial cell; ***Platelet (Figure 3A). Significantly more platelet infiltration was found in allogeneic grafts as compared to syngeneic grafts ($p<0.01$, n=3) (Figure 3B). MP response to anti-cRGD treatment: high-resolution perfusion map (Figure 3C) and average MP of the allogeneic heart myocardium at day 4 post-transplantation (Figure 3D). Animals treated with anti-cRGD demonstrated higher MP than untreated animals (n=3 mice/group, $p<0.05$). Animals were injected with

RAMPS one-day post-transplantation and showed around 90% of platelet reduction one day after injection (Day 0: 0.998×10^7/μL, Day 1: 0.09×10^7/μL, n=5/each group, $p<0.0001$) and the platelet count recovered gradually (Figure 3E). The allogeneic graft perfusion was significantly ($p<0.05$) lower than the syngeneic or the platelet depleted graft perfusion (n=3–5 in each group). No difference was found in MP between the platelet depleted and syngeneic graft (Figure 3F).

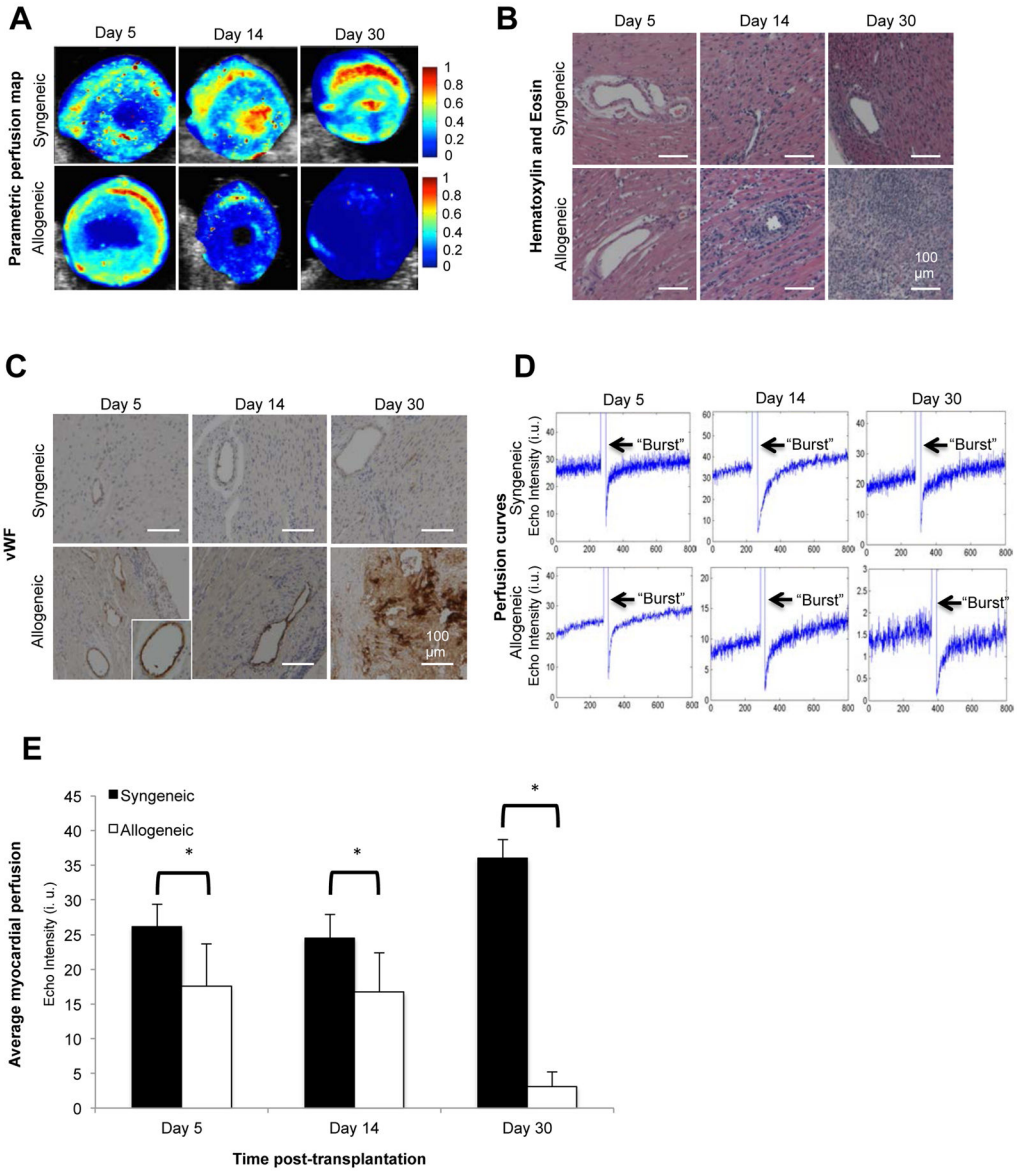

Figure 4. Utility of high-resolution parametric perfusion mapping to detect chronic heart allograft rejection

Parametric perfusion maps of syngeneic and allogeneic grafts on days 5, 14 and 30 post-transplantation show a sharp and progressive decline in the allogeneic grafts over time. On day 30 post-transplantation, minimum MP was noted in the heart allografts as compared to the syngeneic grafts. Red and yellow colors represent higher perfusion (Figure 4A). On day 30 post-transplantation, massive cell infiltrates were noted and the majority of the vessels were filled with thrombi in the allogeneic graft tissue (magnification 20X, scale bar 100 μm) (Figure 4B). Progressive vWF positivity noted in heart allografts over time from day 5 to day 30 post-transplantation (Magnification 20X, scale bar 100 μm) (Figure 4C). As compare to the syngeneic group, the perfusion curves in the allogeneic grafts have a decreasing plateau value over time. The slower slope of the curve in allogeneic grafts indicates the longer time needed for the microbubbles to replenish the imaging plane (as compared to

syngeneic grafts). “Burst” pulses are indicated with arrows. (Figure 4D). The diagram of the average MP in chronic rejection shows the average echo intensities for syngeneic and allogeneic grafts myocardium on days 5, 14, and 30 post-transplantation. A much higher echo intensity unit (i.u.) was observed in the syngeneic groups on each examined day as compared to the allogeneic groups ($p<0.05$, n=3 to 4 mice, echo intensity unit = i.u.) (Figure 4E).